Polyglutamine protein aggregates are dynamic

Soojin Kim*, Ellen A. A. Nollen*, Kazunori Kitagawa†, Vytautas P. Bindokas‡ and Richard I. Morimoto*

**Department of Biochemistry, Molecular Biology and Cell Biology, Rice Institute for Biomedical Research, Northwestern University, Evanston, IL 60208 USA*
†Department of Molecular Pathology, Osaka University Medical School, Suita, Osaka 565, Japan
‡Department of Neurobiology, Pharmacology, and Physiology, The University of Chicago, Chicago, IL 60537, USA
§e-mail: r-morimoto@northwestern.edu

Published online: 30 September 2002; DOI: 10.1038/ncb863

Protein aggregation and the formation of inclusion bodies are hallmarks of the cytopathology of neurodegenerative diseases, including Huntington's disease, Amyotropic lateral sclerosis, Parkinson's disease and Alzheimer's disease. The cellular toxicity associated with protein aggregates has been suggested to result from the sequestration of essential proteins that are involved in key cellular events, such as transcription, maintenance of cell shape and motility, protein folding and protein degradation. Here, we use fluorescence imaging of living cells to show that polyglutamine protein aggregates are dynamic structures in which glutamine-rich proteins are tightly associated, but which exhibit distinct biophysical interactions. In contrast, the interaction between wild-type, but not mutant, Hsp70 exhibits rapid kinetics of association and dissociation similar to interactions between Hsp70 and thermally unfolded substrates. These studies provide new insights into the composite organization and formation of protein aggregates and show that molecular chaperones are not sequestered into aggregates, but are instead transiently associated.

Protein aggregates and inclusions containing Huntingtin protein, superoxide dismutase, α-synuclein, tau or Aβ-peptide are hallmarks of neurodegenerative diseases[1,2]. Immunohistochemical methods and direct biochemical analyses have demonstrated that these aggregates are associated with a variety of cellular proteins, including ubiquitin, components of the proteasome, molecular chaperones (Hsp70, Hsc70, Hdj1 and Hdj2), the cytoskeleton and certain transcription factors (including TBP (TATA binding protein) and CBP (CREB binding protein))[3–11]. Recruitment of TBP and CBP to aggregates is of particular interest, as these proteins contain glutamine stretches of 37 and 18 residues, respectively, and overexpression of CBP was shown to be sufficient to suppress polyglutamine toxicity[12]. Similarly, overexpression of molecular chaperones, such as Hsp70, Hdj1 or Hdj2, has been shown to suppress the toxicity of polyglutamine and α-synuclein aggregates[7,13–15]. These studies have led to an intriguing hypothesis for disease, namely, that the sequestration of certain essential cellular proteins by protein aggregates results in a loss-of-function phenotype that culminates in cellular dysgenesis. In this study, we address the composition and dynamics of polyglutamine protein aggregates and show that glutamine-rich proteins are irreversibly sequestered within aggregates, but exhibit distinct biophysical interactions. By contrast, the interaction between proteins associated with the aggregate and the chaperone Hsp70 is dynamic.

To monitor the dynamics of interactions within polyglutamine aggregates, we generated green fluorescent protein (GFP) fusions with polyglutamine (82Q–GFP and 19Q–GFP) and TBP (TBP–GFP), and a yellow fluorescent protein (YFP) fusion with Hsp70 (Hsp70–YFP). We then monitored the subcellular localization of these proteins when co-expressed with either 82Q–Flag or Htt-150Q (Huntingtin exon1 with an expanded polyglutamine stretch of 150 residues). Expression of 82Q–Flag or Htt-150Q resulted in the formation of cytosolic and nuclear aggregates (Fig. 1a, c, e), whereas expressed 19Q–GFP was soluble and diffuse throughout both compartments (Fig. 1j). The subcellular distribution of TBP–GFP, a nuclear-localized transcription factor, was unaffected by the presence of GFP (Fig. 1k)[16,17]. The molecular chaperone Hsp70 was localized principally to the cytosol of unstressed cells (Fig. 1l) and its chaperone activity was unaffected by the presence of YFP (see Methods). Next, we co-expressed these GFP fusion proteins with the aggregate-inducing 82Q–Flag or Htt-150Q and observed colocalization of 19Q–GFP, TBP–GFP and Hsp70–YFP with the polyglutamine aggregates (Fig. 1a–e). Colocalization of TBP–GFP to the expanded polyglutamine aggregates requires glutamine repeats, as deletion of the amino-terminal region of TBP, which contains 37 glutamine residues, abolished this interaction (Fig. 1f). Similarly, the interaction of Hsp70 with polyglutamine aggregates requires chaperone function, as Hsp70 mutants that lacked either ATPase activity (ATPase mutant) or the substrate binding domain (SBD mutant) showed severely reduced colocalization (Fig. 1g, h)[18]. No such effect was observed when 19Q–CFP was co-expressed with either TBP–YFP or Hsp70–YFP, indicating that the polyglutamine expansion was essential for aggregate formation (data not shown). As the subcellular distribution of GFP alone was unaffected by polyglutamine aggregates (Fig. 1i), we conclude that sequences in 19Q, TBP or Hsp70 are required for association with polyglutamine aggregates.

We then compared the dynamic properties of proteins localized to aggregates using fluorescence recovery after photobleaching (FRAP), a technique that measures the mobility of fluorescent molecules in a living cell[19]. Expression of 82Q–Flag or Htt-150Q was used to initiate the formation of protein aggregates and the fluorescence emitted by 82Q–GFP, 19Q–GFP or TBP–GFP was monitored after photobleaching. FRAP analysis of 82Q–GFP localized to the aggregates demonstrated that 82Q was sequestered there, reducing the mobile fraction to 11% (Fig. 2a, g and Table 1). Similar results were also obtained with aggregates that contained a shorter polyglutamine-expansion of Q40 (data not shown). By comparison, the fluorescence of 19Q–GFP in the cytoplasm was highly mobile, displaying immediate recovery after bleaching (Fig. 2b, g). The diffusion coefficient ($D = 0.66 \pm 0.08$) and mobile fraction of 97% for 19Q–GFP is consistent with its property as a soluble protein (Table 1). In contrast, when 19Q–GFP was associated with 82Q aggregates, mobility was reduced to 33% (Fig. 2c, g and Table 1). Next, we examined the recovery of TBP alone or TBP in cells expressing 82Q–Flag or Htt-150Q. TBP alone displayed 'long-tailed kinetics' (Fig. 2d, g and Table 1). This delay in recovery is probably caused by association of TBP with chromatin and the

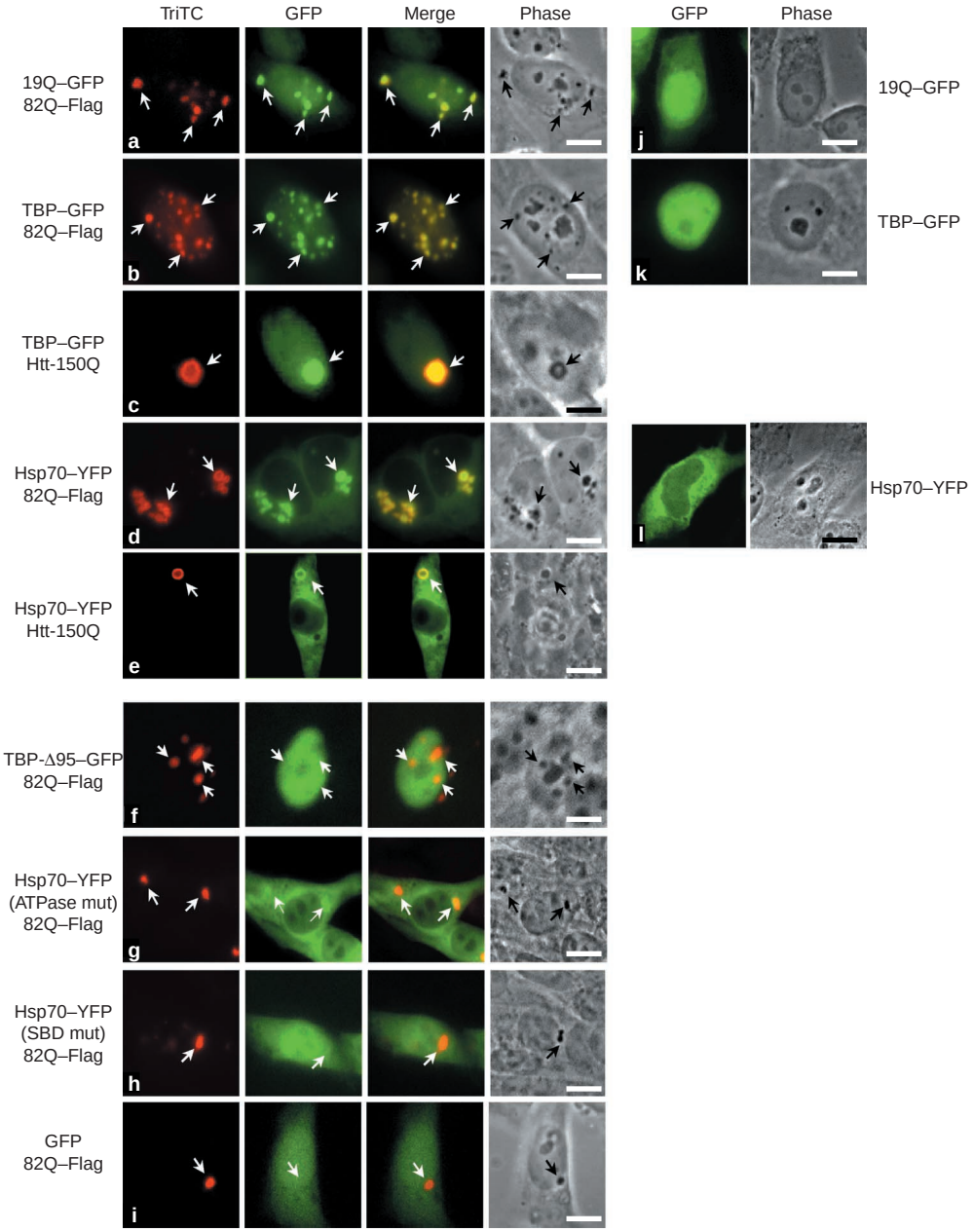

Figure 1 **Colocalization of TBP, 19Q, and Hsp70 fusions with 82Q or Htt-150Q aggregates.** HeLa or O23 cells were cotransfected with constructs encoding either 82Q–Flag or Htt-150Q together with 19Q–GFP (**a**), TBP–GFP (**b**, **c**), Hsp70–YFP (**d**, **e**), TBP-Δ95–GFP (**f**) Hsp70–YFP (ATPase mut (**g**)), Hsp70–YFP (SBD mut (**h**)) or GFP (**i**), as indicated. 82Q–Flag was recognized by a monoclonal antibody to the Flag epitope and Htt-150Q was recognized by HP-1 antibody to the Huntingtin protein. A TriTC-conjugated secondary antibody was used to detect 82Q–Flag and Htt-150Q. Cells expressing 82Q–Flag or Htt-150Q (TriTC, red) and GFP fusion proteins (GFP, green) were visualized by fluorescence microscopy and phase contrast microscopy (Phase). The degree of colocalization was illustrated by merging TriTC and GFP images (Merge). The localization of 19Q–GFP (**h**), TBP–GFP (**i**) or Hsp70–YFP (**j**) alone was visualized, as indicated. Scale bar represents 5 μm.

transcriptional machinery, which can hinder its diffusion[17,20]. Association of TBP with 82Q aggregates markedly reduced the mobile fraction of TBP from 69% to 17% (Fig. 2e, g and Table 1). We observed a similar reduction in the mobility of TBP associated with aggregates containing Htt-150Q (Fig. 2f, g and Table 1), but not Htt-Q21 (data not shown).

Next, we compared the interaction between Hsp70–YFP and 82Q aggregates. We observed a rapid recovery ($D = 0.1 \pm 0.02$), with a mobile fraction of 80% (Fig. 2h, l and Table 1). The mobility of Hsp70 was similar when associated with Htt-150Q-containing aggregates ($D = 0.08 \pm 0.07$, mobile fraction 73%; Fig. 2i, l and Table 1). The rapid mobility of Hsp70 was markedly different from the very slow recovery of glutamine-rich protein interactions with 82Q or Htt-150Q aggregates. The diffusion coefficient for Hsp70, however, was slower than that for soluble 19Q–GFP ($D = 0.66 \pm 0.08$; Table 1). This raises the question as to whether the delay in mobility observed for Hsp70 with polyglutamine aggregates reflects sequestration of the chaperone or an interaction

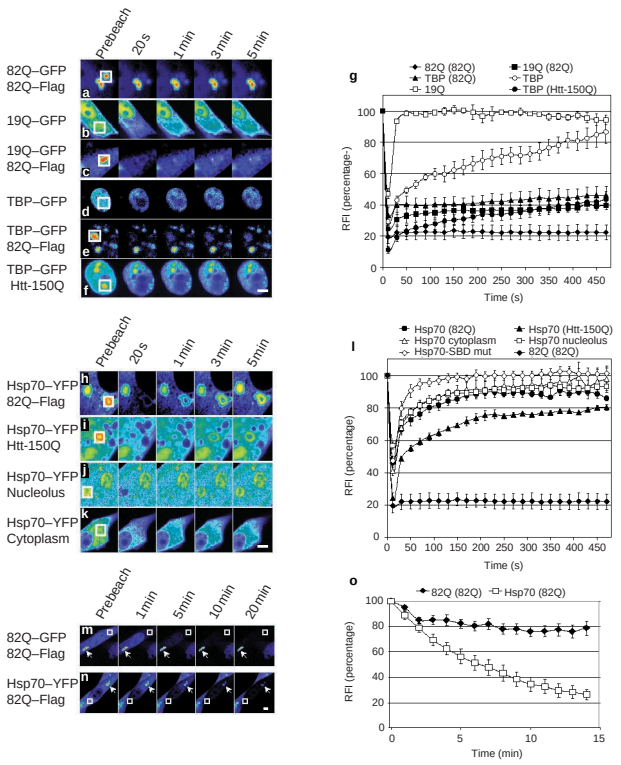

Figure 2 **FRAP and FLIP analysis of polyglutamine aggregates and colocalizing proteins. a–f**, **h–k**, FRAP analysis of the molecular interaction between polyglutamine aggregates and colocalizing proteins. O23 cells were transfected with 82Q–GFP and 82Q–Flag (**a**), 19Q–GFP alone (**b**), 19Q–GFP and 82Q–Flag (**c**), TBP–GFP alone (**d**), TBP–GFP and 82Q–Flag (**e**), TBP–GFP and Htt-150Q (**f**), Hsp70–YFP and 82Q–Flag (**h**), Hsp70–YFP and Htt-150Q (**i**), or Hsp70–YFP alone (**k**). Fluorescent molecules in the boxed area (white box) were subjected to FRAP analysis. **j**, Cells expressing Hsp70–YFP alone were heat-shocked at 45 °C for 30 min and allowed to recover at 37 °C for 1–2 h. Hsp70–YFP that colocalized in the nucleolus (white box) with thermally unfolded substrates was subjected to FRAP analysis. Single scanned images were taken before photobleaching (prebleach) and at the indicated times after photobleaching. Scale bar represents 5 μm. **g**, **l**, Quantitative FRAP analysis of the soluble or the aggregate-associated GFP or YFP fusion proteins. Where indicated, 82Q–Flag or Htt-150Q was used to seed aggregates. The relative fluorescence intensity (RFI) was determined for each time and represented as the average analysis of five cells. Error bars indicate the standard error of the mean (SEM). **m**, **n**, FLIP analysis of 82Q–GFP or Hsp70–YFP associated with 82Q–Flag aggregates. Single scan images were obtained before (Prebleach) and at the indicated times during continuous photobleaching of the boxed area (white box). **o**, Quantitative FLIP analysis of aggregate-associated 82Q–GFP or Hsp70–YFP. Each data point represents the average of five cells. Error bars indicate the SEM.

of Hsp70 with unfolded substrates. As a molecular chaperone, Hsp70 associates with unfolded proteins in the nucleolus of heat-shocked cells[21]. Therefore, we examined the fluorescence recovery and mobile fraction of Hsp70–YFP in the nucleolus ($D = 0.09 \pm 0.1$, mobile fraction 80%) and found these results to be similar to Hsp70–YFP localized to polyglutamine aggregates (Fig. 2j, l and Table 1). To further address whether this decrease in diffusion reflects chaperone–substrate interactions, we examined the cytoplasmic population of Hsp70–YFP. Wild-type Hsp70 ($D = 0.12 \pm 0.01$, mobile fraction 96%) exhibited a similar diffusion to Hsp70 associated with the nucleolus or polyglutamine aggregates (Fig. 2k, l and Table 1). The decreased mobility of Hsp70, relative to 19Q–GFP, required its substrate binding domain, as the Hsp70-SBD mutant ($D = 0.37 \pm 0.05$) exhibited faster diffusion when compared with wild-type Hsp70 (Fig. 2l, Table 1). These data establish that the *in vivo* mobility of wild-type Hsp70–YFP is limited by its substrate interactions and that the colocalization of Hsp70 with polyglutamine aggregates is indistinguishable and indicative of chaperone–substrate interactions, rather than sequestration.

To test directly whether Hsp70 is rapidly released from polyglutamine aggregates, we employed a complementary methodology, fluorescence loss in photobleaching (FLIP), which measures the half-time of colocalized proteins[19]. 82Q–Flag was used to initiate protein aggregate formation and the fluorescence intensity of associated 82Q–GFP or Hsp70–YFP was monitored while a region distant from the protein aggregates was continuously photobleached. If the colocalized protein dissociates from the aggregates, we would expect a loss of fluorescence while an increasing fraction of fluorescent-tagged protein is photobleached. However, if the colocalized protein is stably tethered to the aggregates, the fluorescence intensity should be maintained. FLIP analysis demonstrated that 80% of the initial fluorescent signal persisted over a 14-min period of continuous photobleaching, suggesting that 82Q–GFP is stably associated with the aggregates (Fig. 2m, o). By contrast, Hsp70–YFP fluorescence was rapidly reduced (half-time of 7 min) and continued to decrease to 25% after 14 min (Fig. 2n, o). These results, together with FRAP analysis, show that the interaction of Hsp70 with polyglutamine aggregates represents a process of rapid association and dissociation.

Given the different classes of molecular interactions observed, we wondered if this reflects distinct biophysical states within the structural organization of polyglutamine aggregates. To study the biophysical properties of aggregates, we used fluorescence resonance energy transfer (FRET) microscopy[19]. In cells expressing both 82Q–CFP and 82Q–YFP (Fig. 3), we consistently detected a FRET ratio of 2.5 or more in all protein aggregates. By contrast, in 70% of cells expressing both 82Q–CFP and 19Q–YFP, we detected a range of FRET ratios between 1 and 3 (Fig. 3). This demonstrates an unexpected cell-to-cell heterogeneity in the molecular interactions of the 82Q–CFP/19Q–YFP aggregates. On the basis of this result, we would also expect a variable FRET signal for the interaction of TBP with polyglutamine aggregates. However, when we examined cells co-expressing 82Q–CFP and TBP–YFP, no FRET signal was detected (Fig. 3). The lack of FRET signal for TBP–YFP could be caused by the location of the fluorophore within the chimeric protein. Therefore, FRET experiments were also performed with TBP–YFP constructs in which the YFP moiety was positioned at the N terminus or adjacent to the glutamine-rich region. In all cases, a FRET signal was not observed (data not shown). These data allow us to conclude that the nature of TBP interaction with polyglutamine aggregates is markedly distinct from the molecular interactions observed for 82Q self-association and the variable interactions between 19Q with 82Q. Finally, we examined the interaction between Hsp70–YFP and 82Q–CFP and did not detect any FRET signals (Fig. 3). Together, these data demonstrate that polyglutamine aggregates have heterogeneous molecular interactions with associated proteins and that their biophysical properties are unrelated to the dynamics of these interactions (see Supplementary Information, Fig. S1).

Our study presents a dynamic analysis of the *in vivo* properties of protein aggregates and demonstrates that different classes of proteins which become associated with aggregates exhibit distinct molecular interactions. The relevance to the mechanism of aggregate formation is the entirely unexpected demonstration that Hsp70 binds transiently with the same diffusion coefficient to aggregates as to thermally unfolded substrates. This is in contrast to previous conclusions showing that Hsp70 or glutamine-rich proteins, such as CBP, are sequestered irreversibly by aggregates and that the resulting cellular toxicity is caused by the loss of these proteins for normal cellular function[10,12,13,22]. The results presented here establish that this is not the case and demonstrate that the surface

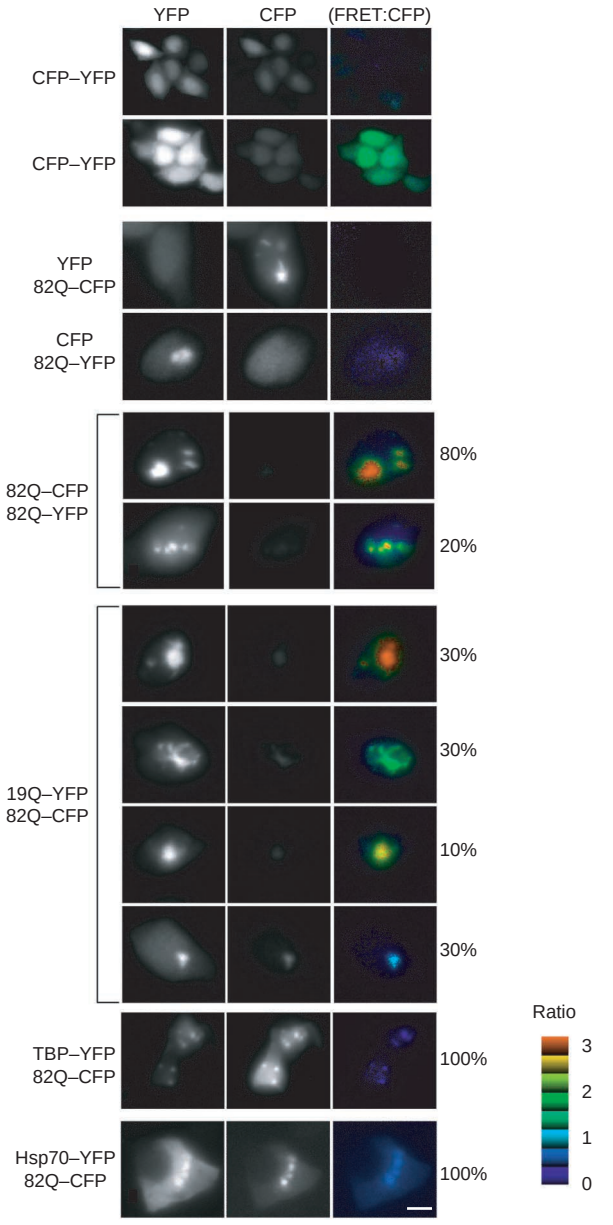

Figure 3 **FRET analysis reveals polymorphic interactions with polyglutamine aggregates.** The nature of biophysical interactions between polyglutamine aggregates and its colocalizing proteins was determined by FRET analysis. We used 82Q–CFP as a donor and YFP fused to 82Q, 19Q, TBP or Hsp70 as the acceptor fluorescence molecules. **a**, In cells co-expressing CFP and YFP, no FRET signal was detected. **b**, In cells co-expressing a chimeric CFP–YFP fusion protein, uniform and intense FRET signal was detected. **c**, **d**, The FRET signal was observed only when both the donor and the acceptor fluorophores were colocalized in the protein aggregates, as co-expressing 82Q–CFP and YFP (and similarly 82Q–YFP and CFP) did not exhibit any FRET signals because neither YFP nor CFP associate with 82Q aggregates. Each panel consists of YFP (yellow), CFP (cyan) and FRET:CFP ratio (pseudo-colour) images of Hela cells expressing 82Q–CFP and 82Q–YFP (**e**, **f**), 19Q–YFP and 82Q–CFP (**g**–**j**), TBP–YFP and 82Q–CFP (**k**), or Hsp70–YFP and 82Q–CFP (**l**). The percentages represent the proportion of cells within the analysed population that exhibited the FRET ratios. The pseudo colour scale indicates the FRET:CFP ratio, ranging from 0 to 3, in which a ratio higher than 1 reflects positive fluorescence energy transfer. Scale bar represents 5 μm.

of the growing aggregate binds and releases Hsp70 in its role as a molecular chaperone to prevent the accumulation of unfolded proteins. Therefore, an explanation for the ability of Hsp70 to suppress protein aggregation of disease-causing proteins may share a common mechanism with the ability of Hsp70, and other chaperones, to suppress the aggregation of unfolded polypeptides induced under a range of environmental and physiological stresses. □

Methods

Plasmid construct cloning

pEF-BOS-F82Q-19, pEGFP-F82Q-19 and pEGFP-F19Q-19 encode 82Q–Flag, 82Q and 19Q fused to GFP, respectively (provided by S. Tsuji, Niigata University, Japan)[23]. CMV–Flag-82Q was generated by inserting a *Not*I/*Sal*I-digested 82Q from pEF-BOS-F82Q-19 into the *Not*I/*Xho*I site of pCDNA3. pCDNA3-Htt150Q was generated by sub-cloning the *Hin*dIII digested Htt with 150Q (provided by M. MacDonald, Harvard University, MA)[24] into *Hin*dIII-digested pCDNA3. To construct pEGFP-N1-TBP, full-length TBP was PCR-amplified from pET-TFIID[25] using 5′ primer, 5′-CGGAATTCGTCATG-GATCAGAACAACAGCCTGCCA-3′, and 3′primer, 5′-CGGGATCCGTCGTCTTCCTGAATCCCTT-TAG-3′, which contain *Eco*RI and *Bam*HI sites, respectively. The stop codon of TBP was mutated to generate a TBP–GFP fusion protein. The PCR product was then subcloned into the *Eco*RI and *Bam*HI sites of pEGFP-N1 (BD Bioscience Clontech, CA). To construct TBP-Δ95–GFP, a fragment of TBP was PCR-amplified from pET-TFIID using 5′ primer, 5′-CCGGAATTCTATGGCAGTGGCAGCTGCAGC-CGTT-3′, which contains an *Eco*RI site, and the 3′ primer used previously to amplify full-length TBP. The PCR product was subcloned into *Eco*RI and *Bam*HI sites of pEGFP-N1. To construct pEYFP-N1-Hsp70, full-length human Hsp70 was PCR-amplified from pET-WT-HSP70 (ref. 18) using 5′ primer, 5′-TCGAATTCTATGGCCAAAGCCGCG-3′ and 3′primer, 5′-GGCGGTACCGTATCTACCTCCTCAAT-3′, which contain *Eco*RI and *Kpn*I sites, respectively. The stop codon of Hsp70 was mutated to generate a Hsp70–YFP fusion protein. The amplified PCR product was then subcloned into *Eco*RI and *Kpn*I sites of pEYFP-N1 (BD Bioscience Clontech, CA).

The chaperone activity of Hsp70–YFP fusion protein was determined, as described[21,26]. Hsp70–YFP containing cells recovered 80% of luciferase activity compared with the cell expressing CFP alone, which exhibited 26% recovery after heat shock. The YFP-fused Hsp70 ATPase domain mutant (Hsp70–YFP-ATPase mut; J. Song, unpublished observations) was generated by PCR-based quick point mutation using a 5′-GTGTTTGACGCGAAGTGGCTGATCGGCCGCAAG-3′ 5′primer and a 5′-CTTGCGGCCGATCAGCCACTTCGCGTCAAACAC-3′ 3′primer to change Arg to Trp at residue 72. The YFP-fused Hsp70 substrate binding domain deletion mutant (Hsp70–YFP-SBD mut) was generated by amplifying the 543-amino-acid sequence of human Hsp70 from pET-WT-HSP70, using 5′primer, 5′-TCGAATTCTATGGCCAAAGCCGCG-3′ and 3′ primer, 5′-CCGCGGTAC-CGTCTCCAGGGCGTTCTTGGCTGACAC-3′, and subcloned into the *Eco*RI and *Kpn*I sites of pEYFP-N1. pECFP-N1-82Q (82Q–CFP), pEYFP-N1-82Q (82Q–YFP), pEYFP-N1-19Q (19Q–YFP) and pEYFP-N1-TBP (TBP–YFP) constructs were generated by subcloning *Eco*RI- and *Bam*HI-digested products from the respective GFP constructs (pEGFP-F82Q-19, pEGFP-F19Q-19 and pEGFP-N1-TBP) into the *Eco*RI and *Bam*HI sites of pECFP-N1 or pEYFP-N1 (BD Bioscience). As a positive control for FRET, a construct encoding a CFP–YFP fusion protein was generated. The CFP gene was PCR-amplified from pECFP-C1 (BD Bioscience) with 5′ primer, 5′-CAGAGCTGGTTTAGTGAACCG-3′ and 3′ primer, 5′-TCGAAGCTTGAGCTCGAGATCTAGTCCGGA-3′, and the amplified PCR product was digested with *Nhe*I and *Bgl*II and subcloned into the *Nhe*I and *Bam*HI site of pEYFP-N1. The resulting CFP–YFP fusion protein contains a nine-amino-acid linker placed between CFP and YFP.

Cell culture and transfection

HeLa cells and O23 cells were grown in DMEM containing 10% fetal bovine serum at 37 °C in 5% CO_2/95% air. Transient transfections were performed using Lipofectamine (Invitrogen, CA) in accordance with the manufacturer's protocol. For colocalization studies, HeLa cells were cotransfected with pEF-BOS-F82Q-19 and pEGFP-N1, pEGFP-F19Q-19, pEGFP-N1-TBP, pEGFP-N1-Δ95-TBP or pEYFP-N1-Hsp70, with a DNA ratio of 7:1. For colocalization of TBP or Hsp70 with Htt-150Q, O23 cells were cotranfected with pcDNA3-htt-150Q and pEGFP-N1-TBP or pEYFP-N1-Hsp70. Finally, for Hsp70 mutant colocalization, O23 cells were cotransfected with CMV–Flag-82Q and Hsp70–YFP(ATPase mut), or Hsp70–YFP (SBD mut). Cells were fixed and analysed 24 h after transfection. For FRAP analysis, O23 cells were grown on 35-mm glass bottom microwell dishes (MatTek Corp., Ashland, MA) and equal amounts of the seeding construct, CMV–Flag-82Q or pCDNA3-htt150Q was cotransfected with pEGFP-F82Q-19, pEGFP-F19Q-19, pEGFP-N1-TBP or pEYFP-N1-Hsp70, as described. After 24 h of transfection, live cells were used for FRAP analysis. For FRET analysis, HeLa cells were transfected with equal amounts of constructs encoding CFP or YFP fusion proteins, as indicated in Fig. 3. Transfected cells were fixed and analysed 24 h after transfection.

Immunofluorescence analysis

Transfected HeLa or O23 cells were fixed in 4% formaldehyde/PBS for 10 min before a 5-min wash in 0.1 M Tris-HCl at pH 8.0. Fixed samples were blocked for 1 h with 10% foetal bovine serum (FBS)/0.3% Triton X-100/PBS at 37 °C. 82Q–Flag was labelled with anti–Flag antibody (M5, 1:500; Sigma, St Louis, MO). Htt-150Q was labelled using HP-1 polyclonal antibody, which recognizes amino acids 80–113 of the Huntingtin protein (provided by M. MacDonald, Harvard University, MA)[24]. After a 1-h incubation, the primary antibodies were detected using trimethyl rhodamine isothiocyanate (TriTC)-conjugated secondary anti-mouse or anti-rabbit antibody (1:100; Sigma). Samples were then mounted in 90% glycerol/2.3% DABCO (diaza-bicyclo-octane) anti-fading solution. Samples were examined by immunofluorescence microscopy with Zeiss Axioscope (Zeiss, Thornwood, NY) and Nikon (Nikon, Millburn, NJ) Optiphot epifluorescence microscopes equipped with an MTI 3CCD camera and IP Lab (Fairfax, VA) spectrum imaging software. The GFP fusion proteins were visualized with XF116-E (GFP) filter sets (Omega Optical, Brattleboro, VT). TriTC-conjugated 82Q–Flag or Htt-150Q was visualized using filter sets for Texas-Red. Adobe Photoshop 5.5 was used for pseudocoloration and merging of the images.

FRAP and FLIP

O23 cells transfected with the constructs for FRAP analysis were maintained at 37 °C for the 1–2-h

Table 1 Quantitative analysis of polyglutamine protein interactions.

Proteins	Localization	D mm² s¹	Mobile fraction
82Q–GFP	82Q aggregate	N/A*	11.0 ± 4.2
TBP–GFP	Nucleus	N/A†	69.4 ± 13.3‡
TBP–GFP	82Q aggregate	N/A*	16.7 ± 10.1
TBP–GFP	Htt-150Q aggregate	N/A*	27.6 ± 10.2
19Q–GFP	Cytoplasm	0.66 ± 0.08	96.6 ± 6.1
19Q–GFP	82Q aggregate	N/A*	32.9 ± 5.0
Hsp70–YFP	Cytoplasm	0.12 ± 0.01	95.9 ± 10.7
Hsp70–YFP	Nucleolus	0.09 ± 0.10	79.9 ± 10.3
Hsp70–YFP	82Q aggregate	0.10 ± 0.02	80.5 ± 7.3
Hsp70–YFP	Htt-150Q aggregate	0.08 ± 0.07	72.6 ± 9.0
Hsp70–YFP SBDmut	Cytoplasm	0.37 ± 0.05	100 ± 3.3

data is a summary of diffusion coefficient (D) and mobile fraction from the FRAP analysis in Fig. 2.

*Diffusion coefficient could not be determined, as the mobile fraction was below 50% and the recovery kinetics did not fit a diffusion profile.

†Diffusion coefficient could not be determined as TBP did not reach $Ne_{(final)}$ during the experiment. ‡Mobile fraction of TBP was estimated using the maximum recovery detected during the experiment.

‡Mobile fraction of TBP was estimated using the maximum recovery detected during the experiment.

duration of the experiment. Photobleaching for FRAP and FLIP analysis was performed as described previously[27], using a Zeiss LSM510 Axiovert confocal microscope and a 40× oil objective lens. For FRAP analysis, a single image was taken at 9th zoom power and an area of 36 μm² was bleached for 10 s (60 iterations), after which time an image was collected every 20 s. For FLIP analysis, a single image was taken at 5th zoom power and an area of 46 μm² was bleached away from aggregates and images were collected after every 1 min (250 iterations) of photobleaching. Relative fluorescence intensity (RFI) was determined using the equation $RFI = (Ne_t/N1_t)/(Ne_0/N1_0)$ equation. Ne_t is the average intensity of the bleached area at a given time point. $N1_t$ is the average intensity of non-bleached area at the corresponding times and functions as a control for general photobleaching and background fluorescence. Ne_0 and $N1_0$ are the average intensity before photobleaching of the bleached or non-bleached area, respectively. For 82Q–GFP, 19Q–GFP and Hsp70–YFP, a non-bleached cytoplasmic area was used as $N1_0$. A non-bleached area in the nucleus was used as $N1_0$ for TBP–GFP analysis. RFI for FLIP analysis was calculated with the above equation, except that Ne_t is the average intensity of an aggregate at a given time point and $N1_t$ is the average intensity of non-bleached area in the neighbouring cell at the corresponding time. The mobile fraction (M_f) was determined as previously described[19,28], using $M_f = (Ne_{(final)} - Ne_0)/(Ne_1 - Ne_0)$, in which $Ne_{(final)}$ is the final intensity after full recovery and Ne_1 is intensity immediately after bleaching. The diffusion coefficient was determined as previously described[29], where a RFI versus time curve was fitted to the equation, $Ne_t = Ne_{(final)}(1 - w^2(w^2 + 4pDt)^{-1})^{1/2}$, where Ne_t is the intensity as a function of time, w^2 is the bleached area and D is the effective one dimensional diffusion coefficient. Graphpad Prism software (GraphPad Software, San Diego, CA) was used to determine the D value that allowed best-fit with earlier time points.

FRET analysis

HeLa cells were grown in a 2-well glass chamber and cotransfected the next day with CFP or YFP fusion constructs, as indicated in the figures. All images were obtained using an Olympus BX50WI (fixed stage, upright), 100× NA1.3 objective equipped with I-penta Max CCD camera (Roper Scientific, Trenton, NJ) and Metamorph software (Universal Imaging Corp., Downington, PA). For each analysis, CFP, YFP and FRET images were taken using the following filter sets (Chroma Technology Corp., Battleboro, VT): CFP filter set, 440-nm excitation and 485-nm emission filters; YFP filter set, 500-nm excitation and 535-nm emission filters; FRET filter set, 440-nm excitation and 535-nm emission filters. The acquired images were then analysed using Metamorph imaging software.

The overlap between the donor (CFP) emission and the acceptor (YFP) excitation spectra, which is required for the efficient energy transfer, contributes to the detection of donor and acceptor fluorescence through the FRET filter set. Consequently, the fluorescence image that is acquired using the FRET filter set consists of both FRET and non-FRET signals. Therefore, we applied the correction algorithm to each image to generate the 'corrected FRET' image, as previously described[30]. To calculate the donor contribution, we acquired CFP and FRET images of HeLa cells that express CFP protein alone. Approximately 15–20 regions of interest (ROI) were assigned to each image and the average pixel intensity per area in both CFP and FRET images was measured. We then plotted the average CFP intensities against the corresponding FRET average and the correction value for CFP was obtained by determining the slope. The correction term for the acceptor contribution was determined by the same method, except YFP and FRET filter sets were used to acquire images of HeLa cells expressing YFP protein alone. We then applied the following algorithm on a pixel-by-pixel basis to the entire image to generate the 'corrected FRET' image:

$FRET^c = FRET - (0.79 \times FRET_{CFP}) - (0.06 \times FRET_{YFP})$.

The FRET ratio image was then generated by calculating the ratio between $FRET^c$ and CFP fluorescence.

RECEIVED 23 APRIL 2002; REVISED 7 JULY 2002; ACCEPTED 3 SEPTEMBER 2002; PUBLISHED 30 SEPTEMBER 2002.

1. Kopito, R. R. & Ron, D. *Nature Cell Biol.* **2,** E207–E209 (2000).
2. Zoghbi, H. Y. & Orr, H. T. *Annu. Rev. Neurosci.* **23,** 217–247 (2000).
3. Perry, G., Friedman, R., Shaw, G. & Chau, V. *Proc. Natl Acad. Sci. USA* **84,** 3033–3036 (1987).
4. Kuzuhara, S., Mori, H., Izumiyama, N., Yoshimura, M. & Ihara, Y. *Acta Neuropathol.* **75,** 345–353 (1988).
5. Davies, S. W. *et al. Cell* **90,** 537–548 (1997).
6. Perez, M. K. *et al. J. Cell Biol.* **143,** 1457–1470 (1998).
7. Cummings, C. J. *et al. Nature Genet.* **19,** 148–154 (1998).
8. Martin, J. B. *N. Engl. J. Med.* **340,** 1970–1980 (1999).
9. Kazantsev, A., Preisinger, E., Dranovsky, A., Goldgaber, D. & Housman, D. *Proc. Natl Acad. Sci. USA* **96,** 11404–11409 (1999).
10. Suhr, S. T. *et al. J. Cell Biol.* **153,** 283–294 (2001).
11. Rajan, R. S., Illing, M. E., Bence, N. F. & Kopito, R. R. *Proc. Natl Acad. Sci. USA* **98,** 13060–13065 (2001).
12. Nucifora, F. C., Jr *et al. Science* **291,** 2423–2428 (2001).
13. Stenoien, D. L. *et al. Hum. Mol. Genet.* **8,** 731–741 (1999).
14. Kobayashi, Y. *et al. J. Biol. Chem.* **275,** 8772–8778 (2000).
15. Auluck, P. K., Chan, H. Y., Trojanowski, J. Q., Lee, V. M. & Bonini, N. M. *Science* **295,** 865–868 (2002).
16. Patterson, G. H., Schroeder, S. C., Bai, Y., Weil, A. & Piston, D. W. *Yeast* **14,** 813–825 (1998).
17. Chen, D., Hinkley, C. S., Henry, R. W. & Huang, S. *Mol. Biol. Cell* **13,** 276–284 (2002).
18. Freeman, B. C., Myers, M. P., Schumacher, R. & Morimoto, R. I. *EMBO J.* **14,** 2281–2292 (1995).
19. Lippincott-Schwartz, J., Snapp, E. & Kenworthy, A. *Nature Rev. Mol. Cell Biol.* **2,** 444–456 (2001).
20. Nagle, J. F. *Biophys J.* **63,** 366–370 (1992).
21. Nollen, E. A. *et al. Proc. Natl Acad. Sci. USA* **98,** 12038–12043 (2001).
22. Paulson, H. L. *Am. J. Hum. Genet.* **64,** 339–345 (1999).
23. Igarashi, S. *et al. Nature Genet.* **18,** 111–117 (1998).
24. Trettel, F. *et al. Hum. Mol. Genet.* **9,** 2799–2809 (2000).
25. Kao, C. C. *et al. Science* **248,** 1646–1650 (1990).
26. Michels, A. A., Nguyen, V. T., Konings, A. W., Kampinga, H. H. & Bensaude, O. *Eur. J. Biochem.* **234,** 382–389 (1995).
27. Chen, D. & Huang, S. *J. Cell Biol.* **153,** 169–76 (2001).
28. Axelrod, D., Koppel, D. E., Schlessinger, J., Elson, E. & Webb, W. W. *Biophys J.* **16,** 1055–1069 (1976).
29. Ellenberg, J. *et al. J. Cell Biol.* **138,** 1193–1206 (1997).
30. Gordon, G. W., Berry, G., Liang, X. H., Levine, B. & Herman, B. *Biophys J.* **74,** 2702–2713 (1998).

ACKNOWLEDGEMENTS
We thank R. Miller (Northwestern University Medical School) and his laboratory for advice and the use of their microscope facility for FRET analysis, S. Gines and M. MacDonald (Harvard University) for generously sharing reagents, C. Jolly, J. Widom, S. Huang and R. Holmgren for advice and comments on the paper, and use of the Cell Imaging Facilities in the Department of Cell and Molecular Biology at Northwestern Medical School and on the Evanston campus of Northwestern University. These studies were supported by grants to R.M. from the National Institutes of Health (NIGMS 38109), the Huntington Disease Society of America Coalition for the Cure, the Hereditary Disease Foundation, a Mechanisms in Aging and Dementia Training Programme from the National Institutes of Aging to S.K., the Netherlands Organization for Scientific Research and an European Molecular Biology Organization Long-Term Fellowship to E.N.
Correspondence and requests for material should be addressed to R.I.M.
Supplementary Information accompanies the paper on www.nature.com/naturecellbiology.

COMPETING FINANCIAL INTERESTS
The authors declare that they have no competing financial interests.